JACS
JOURNAL OF THE AMERICAN CHEMICAL SOCIETY
Article
pubs.acs.org/JACS

A Rhodanine Flanked Nonfullerene Acceptor for Solution-Processed Organic Photovoltaics

Sarah Holliday,*[,†] Raja Shahid Ashraf,[†] Christian B. Nielsen,[†] Mindaugas Kirkus,[†] Jason A. Röhr,[‡,†] Ching-Hong Tan,[†] Elisa Collado-Fregoso,[†] Astrid-Caroline Knall,[†] James R. Durrant,[†,§] Jenny Nelson,[‡] and Iain McCulloch[†,∥]

[†]Department of Chemistry and Centre for Plastic Electronics and [‡]Department of Physics and Centre for Plastic Electronics, Imperial College London, London SW7 2AZ, United Kingdom

[§]SPECIFIC IKC, Swansea University, Baglan Bay Innovation Centre, Port Talbot, Swansea SA12 7AX, United Kingdom

[∥]Physical Sciences and Engineering Division, King Abdullah University of Science and Technology (KAUST), Thuwal, Saudi Arabia 23955−6900

Supporting Information

ABSTRACT: A novel small molecule, **FBR**, bearing 3-ethylrhodanine flanking groups was synthesized as a nonfullerene electron acceptor for solution-processed bulk heterojunction organic photovoltaics (OPV). A straightforward synthesis route was employed, offering the potential for large scale preparation of this material. Inverted OPV devices employing poly(3-hexylthiophene) (P3HT) as the donor polymer and **FBR** as the acceptor gave power conversion efficiencies (PCE) up to 4.1%. Transient and steady state optical spectroscopies indicated efficient, ultrafast charge generation and efficient photocurrent generation from both donor and acceptor. Ultrafast transient absorption spectroscopy was used to investigate polaron generation efficiency as well as recombination dynamics. It was determined that the P3HT:**FBR** blend is highly intermixed, leading to increased charge generation relative to comparative devices with P3HT:$PC_{60}BM$, but also faster recombination due to a nonideal morphology in which, in contrast to P3HT:$PC_{60}BM$ devices, the acceptor does not aggregate enough to create appropriate percolation pathways that prevent fast nongeminate recombination. Despite this nonoptimal morphology the P3HT:**FBR** devices exhibit better performance than P3HT:$PC_{60}BM$ devices, used as control, demonstrating that this acceptor shows great promise for further optimization.

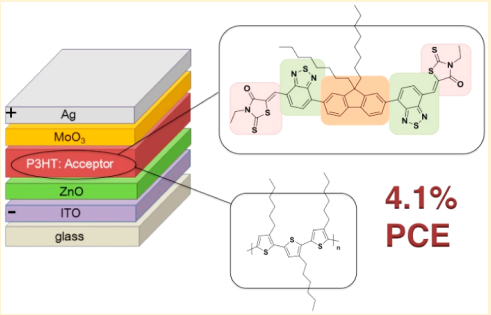

INTRODUCTION

Since the introduction of fullerenes to the field of organic photovoltaics (OPV) in the early 1990s, C_{60} and C_{70} derivatives such as phenyl-$C_{60/70}$ butyric acid methyl ester ($PC_{60/70}BM$) have been the prevailing electron acceptor materials for bulk heterojunction OPV devices.[1,2] The long-lived success of fullerenes arises from their unrivaled electron acceptor properties. These properties include (i) high electron mobility; (ii) delocalization of the lowest unoccupied molecular orbital (LUMO) over the whole surface of the molecule to allow three-dimensional electron transfer and transport; (iii) reversible electrochemical reduction to yield stable reduced charged species; and (iv) formation of domains from solution deposition that are on the appropriate length-scale for charge separation, with both pure and mixed phases created.[3,4] Despite these advantageous properties, however, fullerene acceptors have some limitations. These include (i) weak absorption and poor tunability of absorption over the range of intense regions of the solar spectrum, limiting their contribution to the photocurrent; (ii) morphological instability in thin film blends over time, leading to macroscopic crystallite formation and device failure; (iii) high synthetic costs; and (iv) limited scope for synthetic control over electronic and structural properties.[5,6] For these reasons, research has recently focused on the development of acceptor materials that can be used to replace fullerenes. The most common design involves small molecules with electron deficient units: perylene diimide,[7−10] diketopyrrolopyrrole,[11−13] benzothiadiazole,[14−16] and dicyanovinyl[17−19] being common structural templates. Numerous solution-processable, synthetically versatile and highly absorbing materials have been reported, but the performance in devices generally lags behind that of the fullerenes. Very few nonfullerene acceptors give power conversion efficiencies over 3%, even with high performance donor polymers, and fewer still can exceed the comparison device with fullerene.[20−23] Furthermore, synthesis of these materials is frequently lengthy and low yielding, and thus offers little advantage over fullerenes in terms of synthetic scalability, an important aim for the production of cheap and printable solar cells.

Received: November 4, 2014
Published: December 25, 2014

DOI: 10.1021/ja5110602
J. Am. Chem. Soc. 2015, 137, 898−904

The small molecule **FBR** (Scheme 1) was designed to be synthetically simple and versatile, with wide scope to modify

Scheme 1. Synthesis of Rhodanine Flanked Acceptor FBR

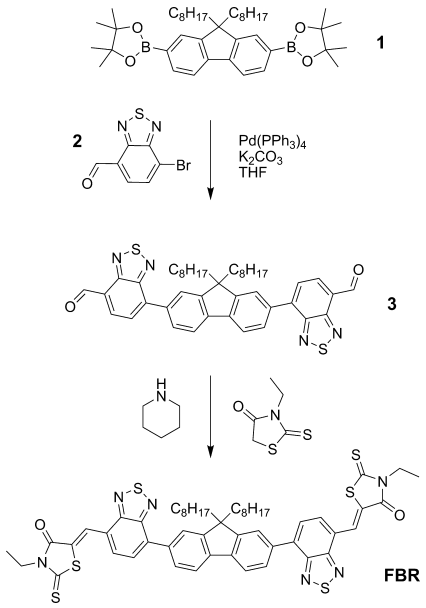

the structural, electronic, and morphological properties through chemical design. Fluorene was chosen as a rigid aromatic core to facilitate transport and preserve conjugation along the length of the molecule, which allows versatile energy level tuning as well as offering the potential to vary the pendant alkyl chains to tune the solubility and crystallinity. Incorporation of benzothiadiazole extends the conjugation, thus improving charge transport, as well as affording electron deficient character to the outside of the molecule. To cap the ends of the molecule, 3-ethylrhodanine was chosen as an electron withdrawing flanking group. Rhodanine derivatives are commonly used in dye chemistry for the creation of strong push−pull chromophores,[24−26] and recently in the field of OPV there have been several high performance small molecule donors published bearing rhodanine groups.[27−30] There are very few reports, however, of rhodanine units being used in the capacity of the acceptor material.[31] As well as affording electron withdrawing character to the periphery of the molecule via its ketone and thioketone groups, rhodanine allows for the further control over solubility by altering the imide alkyl chain. In this paper, the ethyl group is employed in order to inhibit the hydrogen bonding associated with the unalkylated rhodanine. This increases the solubility in common organic solvents while avoiding overly bulky alkyl groups on the periphery of the molecule. In order to facilitate electron transfer, the molecule was designed to have solubilizing alkyl chains on the electron-rich center of the molecule in order to leave the outer, electron-withdrawing portion of the molecule sterically available as is the case in fullerene molecules.

RESULTS AND DISCUSSION

Materials Synthesis and Optoelectronic Properties. The synthesis of **FBR** is documented in the Supporting Information and summarized in Scheme 1. Suzuki coupling of 9,9-dioctylfluorene-2,7-diboronic acid pinacol ester **1** with bromo-2,1,3-benzothiadiazole-4-carboxaldehyde **2** afforded the aryl dialdehyde intermediate **3**. Subsequent Knoevenagel condensation with 3-ethylrhodanine yielded the product **FBR**. The material is thermally stable up to ca. 300 °C as confirmed by thermogravimetric analysis (see the Supporting Information) and soluble in common organic solvents such as chloroform and toluene. Although the synthesis is reported on a small (laboratory) scale, all of the precursor materials are relatively inexpensive and the reactions are sufficiently straightforward that larger scale production should be easily possible. This demonstrates an important advantage over fullerenes, as well as many nonfullerene acceptors for which multistep syntheses are often required.

Density functional theory (DFT) calculations were carried out on the molecular structure using Gaussian at the B3LYP/6-31G* level of theory. Figure 1 illustrates that the highest

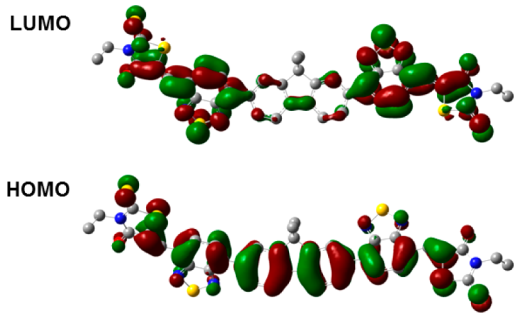

Figure 1. Minimum energy conformation of **FBR** (with methyl replacing octyl groups) calculated using Gaussian (B3LYP/6-31G*) to visualize the LUMO and HOMO distribution.

occupied molecular orbital (HOMO) of **FBR** is delocalized over the whole molecule, while the lowest unoccupied molecular orbital (LUMO) is concentrated onto the more electron deficient periphery. It is expected that this large electron-accepting area on the outer, sterically exposed part of the molecule will benefit charge transfer. Meanwhile the molecular oscillator strength, and thus the extinction coefficient, should benefit from the extent of overlap between HOMO and LUMO.

UV−vis absorption spectroscopy (Figure 2) reveals a maximum absorption of **FBR** at 488 nm in solution and 509 nm in the thin film. Compared with the maximum absorption of $PC_{60}BM$ (ca. 300 nm), **FBR** absorbs in a region of the

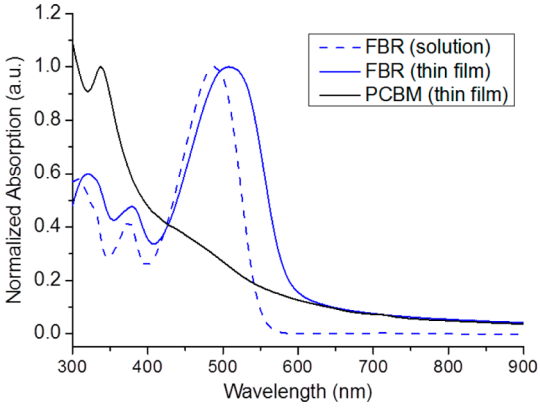

Figure 2. Normalized UV−vis absorption spectra of **FBR** in chloroform solution compared with the thin film absorption (spun from chloroform solution) of **FBR** and $PC_{60}BM$.

DOI: 10.1021/ja5110602
J. Am. Chem. Soc. 2015, 137, 898−904

Table 1. Optoelectronic Properties of FBR and $PC_{60}BM$

	λ_{max} (nm)[a]	ε (10^4 M^{-1} cm^{-1})[b]	E_g^{opt} (eV)[a]	E_g^{elec} (eV)[c]	HOMO (eV)[c]	LUMO (eV)[c]
FBR	509	3.46	2.14	2.14	−5.70	−3.57
$PC_{60}BM$	300	0.49	1.75	2.06	−5.87	−3.84

[a]Measured in thin film, spin-cast from 5 mg/mL chloroform solution. [b]Measured in chloroform solution. [c]Measured by cyclic voltammetry in dichloromethane solution with tetrabutylammonium hexafluorophosphate electrolyte.

spectrum with much higher solar flux[32] which offers a great advantage in terms of contributing to the photocurrent via absorption. Figure 2 shows a normalized UV−vis absorption spectra, while Table 1 shows that the extinction coefficient of **FBR** at its maximum absorption wavelength, measured in solution, is 1 order of magnitude greater than that of $PC_{60}BM$ at its maximum absorption wavelength in the visible region. Due to the high degree of symmetry of $PC_{60}BM$, many of the low energy transitions are forbidden which severely limits absorption in the visible region.[33,34] This further demonstrates the capacity for this small molecule to yield a greater photocurrent than C_{60} fullerene acceptors.

The electrochemical behavior of the acceptors was studied by cyclic voltammetry (CV) in dichloromethane solution. The reduction cycle of **FBR** is shown in Figure 3 in comparison with

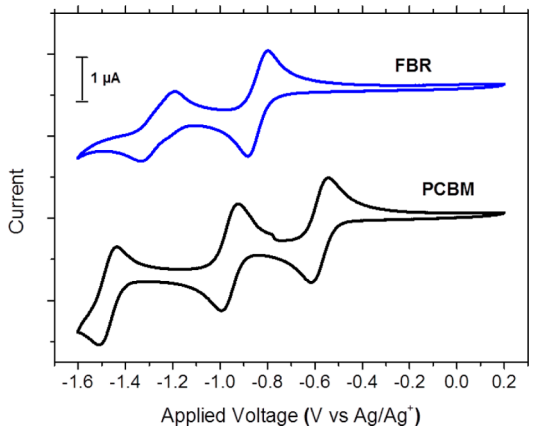

Figure 3. First reduction cycles of **FBR** and $PC_{60}BM$ measured by cyclic voltammetry in dichloromethane solution with tetrabutylammonium hexafluorophosphate electrolyte.

that of $PC_{60}BM$. Within the reduction limits of the solvent, **FBR** undergoes at least two reversible reduction events. Reversibility demonstrates that the reduced species is not electrochemically unstable which is important for the operational stability of devices, while the presence of more than one reduction event shows that there are multiple low-lying excited states, a property which has previously been observed to facilitate charge separation.[35] The HOMO and LUMO values were calculated from the onset voltages of oxidation and reduction, respectively, as presented in Table 1. It may be noted that the electrochemical bandgap measured by these methods corresponds well with the optical bandgap measured from the onset of absorption in the thin film. The LUMO energy of **FBR** (−3.57 eV) is relatively low due to the presence of strong electron withdrawing units, but higher lying than that of $PC_{60}BM$ (−3.84 eV). In order to maximize the achievable V_{oc}, it is desirable that the LUMO level of the acceptor is as high-lying as possible while still allowing for electron transfer from the donor. It is generally assumed that the minimum LUMO−LUMO offset required for efficient electron transfer is at least 0.2 eV.[36] **FBR** fulfills this requirement for wide bandgap polymers such as poly(3-hexylthiophene) (P3HT), with an improved V_{oc} expected relative to $PC_{60}BM$ due to the higher lying LUMO.

Structural Properties. To study the structural properties of the new acceptor, differential scanning calorimetry (DSC) and X-ray diffraction (XRD) were performed on the neat material, the results of which are shown in Figure 4. On the first heating

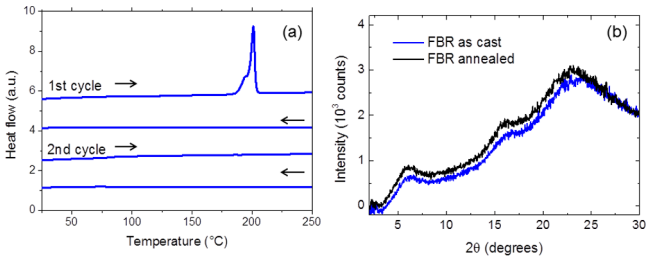

Figure 4. (a) DSC thermogram of **FBR** upon first and second heating and cooling cycles, measured at 10 °C/min under nitrogen. (b) XRD of neat **FBR** film dropcast from chlorobenzene, as cast (blue) and annealed (black) at 110 °C for 15 min in air.

cycle by DSC (Figure 4a), a sharp melting endothermic transition is observed at around 200 °C which signifies some degree of molecular order within the bulk material. A broad shoulder is present in the onset of the melt, indicating the possible presence of conformational polymorphs. After melting, the material then appears to become kinetically trapped in the amorphous phase, with no recrystallization observed upon cooling and a featureless second heating and cooling cycle consistent with an amorphous material. XRD data supports the observation that dropcast films of **FBR** are amorphous even after annealing, given that there are no reflections consistent with crystallinity on the length scale of the measurement's accuracy.

The amorphous nature of **FBR** can be understood with reference to the molecular structure of **FBR** as modeled using Gaussian (B3LYP/6-31G*). A large dihedral angle of 35° is calculated between the fluorene core and the benzothiadiazole unit as shown in Figure 5, giving the molecule a nonplanar 3D structure overall. It may be expected that this nonplanar nature would act favorably to prevent the growth of large acceptor domains. One of the major problems with nonfullerene acceptor units such as perylene diimides is the strong tendency to crystallize. This leads to difficulties in controlling the nanostructure of the bulk heterojunction which can result in self-trapping of excitons and, ultimately, poor device performance. There is increasing evidence that nonplanar acceptors perform better than their planar counterparts for this reason.[9,10,37,38] Furthermore, the twisted nature of **FBR** should hypothetically provide the potential for charge transport in more than one dimension, making it more analogous to the fullerenes with their relatively isotropic transport.

DOI: 10.1021/ja5110602
J. Am. Chem. Soc. 2015, 137, 898−904

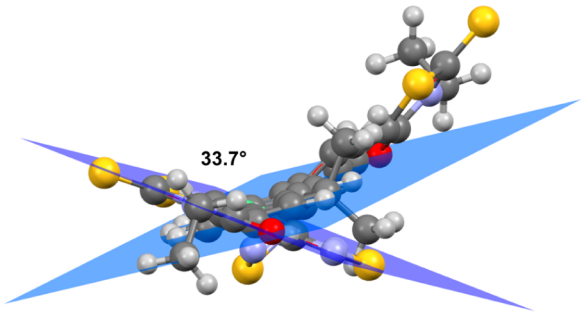

Figure 5. Dihedral planes of **FBR** from the minimum energy conformations calculated using Gaussian (B3LYP/6-31G*).

OPV Device Fabrication and Evaluation. To evaluate the potential of the rhodanine flanked acceptor in bulk heterojunction solar cells, devices were prepared with P3HT as the donor polymer. As well as being one of the most thoroughly studied and understood polymers in the field of organic photovoltaics, P3HT has the potential to be synthesized via low cost and high throughput methods, [39] making it a promising donor partner. Furthermore, P3HT:$PC_{60}BM$ blends provide a good benchmark for comparison of device data. An inverted architecture was chosen for the devices due to the improved environmental stability and ease of fabrication over conventional architectures.[40,41] Devices were fabricated with the configuration glass/ITO/ZnO/P3HT:acceptor (1:1)/MoO_3/Ag. The active layers were deposited by spin-coating from $CHCl_3$:o-DCB (4:1) under ambient conditions, while annealing (15 min at 110 °C), electrode deposition, and device testing were carried out in an inert environment. For comparison, P3HT:$PC_{60}BM$ devices were fabricated in parallel, according to previously optimized procedures. In comparison to P3HT:$PC_{60}BM$, optimum performance for P3HT:**FBR** devices was obtained for thinner photoactive layer and more modest thermal annealing. Full device fabrication details, along with solvent concentrations and blend ratio optimization details, are given in the Supporting Information. Figure 6 shows the current density−voltage (J−V) characteristics for devices with P3HT as the donor and **FBR**/$PC_{60}BM$ as the acceptor, measured under simulated AM1.5G illumination at 100 mW cm^{-2}. The photovoltaic device properties are summarized in Table 2. The **FBR** device

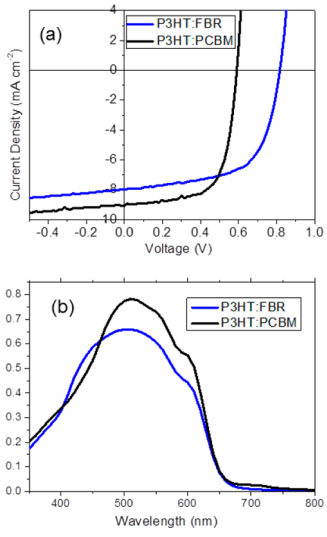

Figure 6. (a) J−V curves and (b) EQE spectra of P3HT:**FBR** (blue) and P3HT:$PC_{60}BM$ (black) devices.

Table 2. Summarized Photovoltaic Characteristics of P3HT:acceptor (1:1) Devices

	J_{sc} (mA cm^{-2})	V_{oc} (V)	FF	PCE (%)
P3HT:**FBR**	7.95	0.82	0.63	4.11
P3HT:$PC_{60}BM$	9.07	0.59	0.66	3.53

produces a lower short circuit current (7.95 mA cm^{-2}) than the fullerene device, which may be partially accounted for by the difference in thickness between devices. A range of thicknesses were evaluated, with an optimal thickness of 80 nm found for the P3HT:**FBR** active layers. The best P3HT:$PC_{60}BM$ devices were thicker with active layers of ca. 150 nm which is one reason for the higher photocurrent. The lower J_{sc} of the P3HT:**FBR** device is, however, offset by the improved open circuit voltage (0.82 V) which is attributed to the higher lying LUMO of **FBR** relative to $PC_{60}BM$. This results in a PCE of 4.11%, which is currently among the highest efficiencies for nonfullerene based devices with P3HT. It also clearly outperforms the comparison $PC_{60}BM$ cell with PCE of 3.53%.

From Figure 6b, it can be seen that the maximum EQE intensity for P3HT:**FBR** devices is 65% at ca. 500 nm, but the EQE profile illustrates how the largely overlapping absorption profiles of polymer and acceptor limit the amount of photocurrent that can be harvested across the spectrum. It is anticipated that by replacing P3HT with a polymer of complementary absorption to **FBR**, a greater photocurrent could be obtained, offering the possibility for even higher device efficiencies with this acceptor. It is noted that the EQE of the P3HT:$PC_{60}BM$ device is higher even at 510 nm, where both P3HT and **FBR** have their peak absorption. This is likely due to the increased thickness of the P3HT:$PC_{60}BM$ films, as well as the greater degree of crystallinity in the P3HT as these devices were annealed for longer and at a higher temperature.

Charge Separation and Recombination Dynamics. Photoluminescence quenching (PLQ) experiments were carried out on P3HT:**FBR** and P3HT:$PC_{60}BM$ blend films as well as neat films, as shown in Figures 7 and Supporting

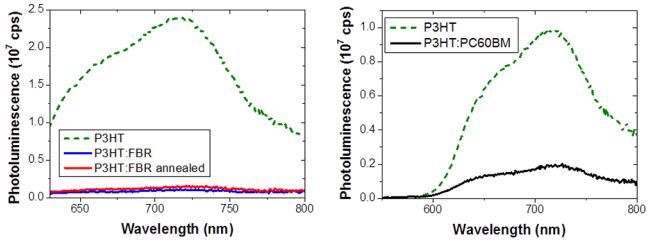

Figure 7. Photoluminescence quenching efficiency of P3HT in (a) P3HT:**FBR** blend and annealed P3HT:**FBR** blend (100 °C 15 min) excited at 600 nm; (b) P3HT:$PC_{60}BM$ blend excited at 532 nm.

Information Figure S8. For the P3HT:**FBR** blend film, both P3HT and **FBR** photoluminescence is strongly quenched (96% and 99%) respectively, indicative of efficient exciton separation following excitation of either donor or acceptor. This is consistent with the film energetics that constitute a Type II heterojunction, which is efficient in both electron and hole transfer. Thermal annealing resulted in modest reduction in

DOI: 10.1021/ja5110602
J. Am. Chem. Soc. 2015, 137, 898−904

PLQ from both P3HT and **FBR** (by 93 and 95%, respectively), indicating that this thermal annealing drives a modest increase in the phase segregation of donor and acceptor. This PLQ remains relatively strong compared to P3HT:$PC_{60}BM$, where the P3HT emission is only quenched by 80% (see Figure 7b). This relatively modest PLQ in P3HT:$PC_{60}BM$ blends has been correlated with strong phase segregation in this blend,[42] resulting in the formation of pure P3HT domains on the 5–10 nm length scale. The higher PLQ for the P3HT:**FBR** is indicative of a more intimately mixed blend morphology.

The charge generation process was measured with ultrafast transient absorption spectroscopy. Transient spectra are shown in the Supporting Information (Figure S9). Figure 8a shows the

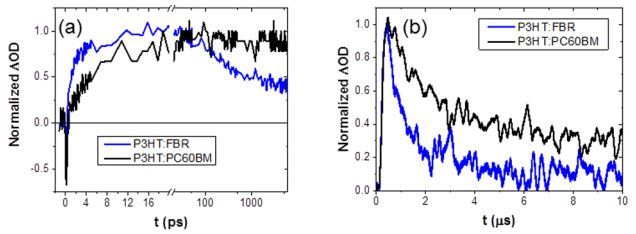

Figure 8. Rise and decay of P3HT:**FBR** and P3HT:$PC_{60}BM$ blend polaron signals using transient absorption spectroscopy under same excitation density and atmosphere (4 μJ cm^{-2}, N_2) (a) in picosecond time scale, excited at 600 nm and probed at 725 nm, and (b) in microsecond time scale, excited at 532 nm and probed at 980 nm.

transient data at a probe wavelength of 725 nm, employing selective excitation of P3HT at 600 nm. The 725 nm wavelength corresponds to the P3HT PL maximum; at this probe wavelength, initially excited P3HT excitons show a negative signal (assigned to stimulated emission) while P3HT polarons exhibit a positive signal. For the P3HT:$PC_{60}BM$, the rise time of the initially negative signal at 725 nm, assigned to photoinduced charge separation from P3HT excitons, is clearly biphasic, with an instrument response limited phase and slower phase (exponential time constant of 6 ps). The fast phase is assigned, as previously,[43] to a faster charge separation from P3HT excitons generated in close proximity to $PC_{60}BM$. The slow phase, meanwhile, is assigned to exciton diffusion limited charge separation from excitons generated within pure P3HT domains. For P3HT:**FBR**, the rise kinetics are significantly faster, and dominated by an instrument response limited rise, consistent with the more intimate blend mixing indicated by the PLQ data shown in Figure 7.

Our PLQ and ultrafast transient absorption data indicate that exciton quenching and polaron formation is faster and more efficient in P3HT:**FBR** than P3HT:$PC_{60}BM$. However, the P3HT:**FBR** blend also exhibits faster charge recombination losses than P3HT:$PC_{60}BM$. This is apparent in the ~200 ps decay phase observed in Figure 8a, which has been tentatively assigned to a geminate recombination process. It is also apparent on longer (microsecond) time scale transient absorption data, as shown in Figure 8b, which show faster decay dynamics for P3HT:**FBR** blends, indicative of faster nongeminate recombination. These faster recombination losses are also indicative of a more intermixed blend morphology with **FBR** as the acceptor, although we note that the increased geminate recombination losses may also result from the smaller LUMO–LUMO energy offset for P3HT:**FBR** compared to P3HT:$PC_{60}BM$. An in depth analysis of these recombination losses will be presented elsewhere. The faster nongeminate recombination losses of P3HT:**FBR** are consistent with a thinner photoactive thickness for optimum device efficiency (with faster recombination increasing losses during charge transport). They are also consistent with the increase in V_{OC} in **FBR** devices relative to $PC_{60}BM$ being less than the decrease in electron affinity (as faster recombination losses reduce V_{OC}).[44]

Microsecond transient absorption data employing relatively selective P3HT or **FBR** excitation (at 532 and 355 nm, respectively) resulted in equivalent yields of long-lived polarons per absorbed photons (Figure S10). This confirms efficient charge generation from both P3HT and **FBR** excitons, consistent with our PLQ and EQE data.

Electron Mobility Measurements. The electron mobility of **FBR** was determined from space-charge-limited current (SCLC) measurements,[45] where the active layer blend was sandwiched between two electron selective contacts, namely, ITO/TiO_2 and Ca/Al. The electron mobility of the P3HT:**FBR** blend was then compared to a similar device with a P3HT:$PC_{60}BM$ blend. The blend thicknesses were measured using a profilometer. The current density was measured between −5 and 5 V in steps of 0.05 V, and the resulting J–V curves were fitted using a numerical solver,[46] where the charge carrier mobility, the injection barrier heights and the trap density was allowed to vary. The resulting J–V curves are shown for forward bias on a log–log scale in Figure 9. It is

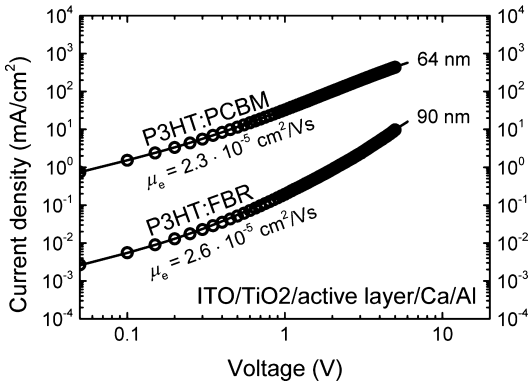

Figure 9. Space-charge-limited current density–voltage curves of electron only devices (black circles) and numerical fits (black lines) of P3HT:$PC_{60}BM$ and P3HT:**FBR** blends.

common to fit to SCLC data with the Mott–Gurney square law, but the assumptions made to derive the equation are generally not true for thin devices, and the equation fails especially in the case of traps.[47] For this reason, a novel approach of numerical fitting is used.[48] The two blends were found to yield similar values for the electron mobilities, with μ_e = 2.3 × 10^{-5} $cm^2/(V\ s)$ and μ_e = 2.6 × 10^{-5} $cm^2/(V\ s)$ for P3HT:$PC_{60}BM$ and P3HT:**FBR**, respectively. The injection barrier heights (which were found to be similar for both injection from TiO_2 and Ca) were found to be 0.093 eV for P3HT:$PC_{60}BM$, and since a similar contacting scheme was used for both blends, similar injection barrier heights were assumed for P3HT:**FBR** since charge injection from the contact into the polymer is assumed. Extended states in the form of exponential tails into the band gap has previously been reported in polymer:fullerene blends.[49] Where the devices with P3HT:$PC_{60}BM$ showed intrinsic behavior, the P3HT:**FBR** showed trap behavior so that exponential tails were needed in order to fit to the data (N_T = 5.2 × 10^{18} cm^{-3} with $E_{ch} = 2k_BT$,

DOI: 10.1021/ja5110602
J. Am. Chem. Soc. 2015, 137, 898–904

where N_T is the density of the exponential states and E_{ch} the characteristic energy of the exponential tail),[50] which is the reason for the low observed current density despite the similar electron mobility. The difference in the trap nature of the two blends can be attributed to the amorphous nature of **FBR** and the crystalline nature of the P3HT. It should be noted that even though trap states were not observed in the case of P3HT:PC_{60}BM, a low concentration could still be present which would not manifest in the SCLC measurements.

Morphological Stability. In order to compare the morphological stability of our P3HT:acceptor blends, films were spin-cast using the same active layer solutions as used in device preparation, and these were heated to 140 °C for a period of several hours. Optical microscopy was used to observe the formation of any micrometer-scale aggregation (Figure 10). In agreement with previous studies,[51] the

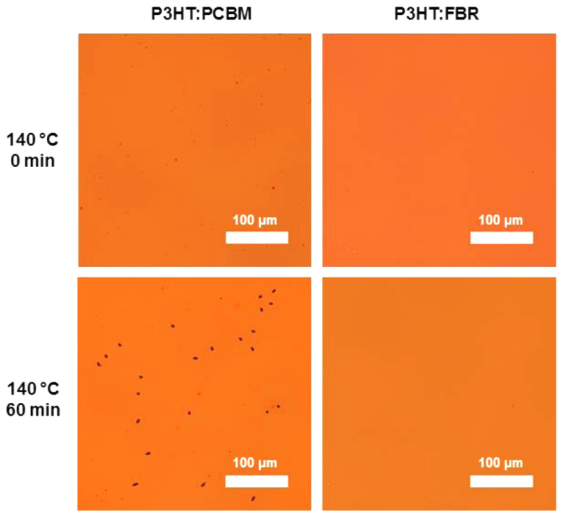

Figure 10. Morphological stability of P3HT:acceptor films studied by optical microscopy. Films were annealed in air at 140 °C, and the images shown are after 0 and 1 h.

P3HT:PC_{60}BM film formed relatively large fullerene clusters within 1 h of annealing. By contrast, no particles were visible in the P3HT:**FBR** films after annealing even for 12 h. Previous reports of fullerene aggregation have correlated such optical micrograph images with atomic force microscopy (AFM) and TEM results and a corresponding degradation in solar cell performance.[52] It is possible, in this respect, that the reduced aggregation demonstrated by the rhodanine flanked acceptor should be advantageous in terms of device stability.

CONCLUSIONS

In summary, a novel rhodanine flanked small molecule **FBR** was synthesized and its potential as an electron acceptor is demonstrated. The material is structurally simple and can be synthesized in high yields via relatively few synthetic steps. This gives our molecule an intrinsic advantage over fullerene acceptors, for which high cost and lengthy purification techniques have long been a prohibitive factor. Furthermore, this molecule is highly absorbing in the visible region, offering the potential for enhanced photocurrent generation in OPV devices. **FBR** demonstrates several advantageous properties for OPV applications. These include reversible reduction behavior with the ability to reversibly accept at least two electrons. Second, the molecule has a nonplanar molecular structure which may help deliver nonanisotropic electron transport, as well as a reduced tendency to crystallize which helps to prevent large crystalline domains from forming in the bulk heterojunction blend composition over extended lifetimes. A higher-lying LUMO energy relative to PC_{60}BM also helps to achieve a high open circuit voltage. The acceptor is effective with P3HT, which is one of the most inexpensive and widely used polymers in the field of OPV and a strong candidate for OPV commercialization. Effective quenching of photoluminescence is observed for this blend, as well as electron mobilities that are comparable to those observed for the P3HT:PC_{60}BM device. It appears from transient absorption measurements that the system is highly intermixed, leading to increased charge generation but faster geminate recombination relative to P3HT:PC_{60}BM devices. Despite this suboptimal morphology, it significantly outperforms the comparison P3HT:PC_{60}BM device. Lateral diffusion of the acceptor appears to be reduced for this acceptor relative to fullerenes, offering the potential for improved morphological stability in devices. Lastly, the P3HT:**FBR** device is well-suited to the inverted device architecture, which offers further stability in terms of reduced reactivity of the electrodes and interlayers relative to conventional architectures.

ASSOCIATED CONTENT

Supporting Information

Complete experimental section including synthetic procedures, device fabrication details, additional photoluminescence and transient absorption spectra, electron mobility measurement details, and atomic force micrographs. This material is available free of charge via the Internet at http://pubs.acs.org.

AUTHOR INFORMATION

Corresponding Author

s.holliday@imperial.ac.uk

Notes

The authors declare no competing financial interest.

ACKNOWLEDGMENTS

We thank BASF for partial financial support, as well as EPSRC (EP/G037515/1) and EPSRC (EP/L016702/1), and EC FP7 Projects X10D (287818) and Nanomatcell (308997) for financial support. A.-C.K. acknowledges the Austrian Science Fund (FWF):[T 578-N19] for financial support.

REFERENCES

(1) Li, C.-Z.; Yip, H.-L.; Jen, A. K. Y. *J. Mater. Chem.* **2012**, *22*, 4161.
(2) Li, G.; Zhu, R.; Yang, Y. *Nat. Photonics* **2012**, *6*, 153.
(3) Treat, N. D.; Brady, M. A.; Smith, G.; Toney, M. F.; Kramer, E. J.; Hawker, C. J.; Chabinyc, M. L. *Adv. Energy Mater.* **2011**, *1*, 82.
(4) Ma, W.; Tumbleston, J. R.; Wang, M.; Gann, E.; Huang, F.; Ade, H. *Adv. Energy Mater.* **2013**, *3*, 864.
(5) Eftaiha, A. a. F.; Sun, J.-P.; Hill, I. G.; Welch, G. C. *J. Mater. Chem. A* **2014**, *2*, 1201.
(6) Lin, Y.; Zhan, X. *Mater. Horiz.* **2014**, *1*, 470.
(7) Sharenko, A.; Proctor, C. M.; van der Poll, T. S.; Henson, Z. B.; Nguyen, T.-Q.; Bazan, G. C. *Adv. Mater.* **2013**, *25*, 4403.
(8) Jiang, W.; Ye, L.; Li, X.; Xiao, C.; Tan, F.; Zhao, W.; Hou, J.; Wang, Z. *Chem. Commun.* **2014**, *50*, 1024.
(9) Rajaram, S.; Shivanna, R.; Kandappa, S. K.; Narayan, K. S. *J. Phys. Chem. Lett.* **2012**, *3*, 2405.
(10) Li, H.; Earmme, T.; Ren, G.; Saeki, A.; Yoshikawa, S.; Murari, N. M.; Subramaniyan, S.; Crane, M. J.; Seki, S.; Jenekhe, S. A. *J. Am. Chem. Soc.* **2014**, *136*, 14589.

DOI: 10.1021/ja5110602
J. Am. Chem. Soc. 2015, 137, 898−904

(11) Lin, Y.; Li, Y.; Zhan, X. *Adv. Energy Mater.* **2013**, *3*, 724.
(12) Lin, Y.; Cheng, P.; Li, Y.; Zhan, X. *Chem. Commun.* **2012**, *48*, 4773.
(13) Patil, H.; Zu, W. X.; Gupta, A.; Chellappan, V.; Bilic, A.; Sonar, P.; Rananaware, A.; Bhosale, S. V.; Bhosale, S. V. *Phys. Chem. Chem. Phys.* **2014**, *16*, 23837.
(14) Schwenn, P. E.; Gui, K.; Nardes, A. M.; Krueger, K. B.; Lee, K. H.; Mutkins, K.; Rubinstein-Dunlop, H.; Shaw, P. E.; Kopidakis, N.; Burn, P. L.; Meredith, P. *Adv. Energy Mater.* **2011**, *1*, 73.
(15) Bloking, J. T.; Han, X.; Higgs, A. T.; Kastrop, J. P.; Pandey, L.; Norton, J. E.; Risko, C.; Chen, C. E.; Brédas, J.-L.; McGehee, M. D.; Sellinger, A. *Chem. Mater.* **2011**, *23*, 5484.
(16) Douglas, J. D.; Chen, M. S.; Niskala, J. R.; Lee, O. P.; Yiu, A. T.; Young, E. P.; Fréchet, J. M. J. *Adv. Mater.* **2014**, *26*, 4313.
(17) Fang, Y.; Pandey, A. K.; Nardes, A. M.; Kopidakis, N.; Burn, P. L.; Meredith, P. *Adv. Energy Mater.* **2013**, *3*, 54.
(18) Zhou, T.; Jia, T.; Kang, B.; Li, F.; Fahlman, M.; Wang, Y. *Adv. Energy Mater.* **2011**, *1*, 431.
(19) Nielsen, C. B.; Voroshazi, E.; Holliday, S.; Cnops, K.; Rand, B. P.; McCulloch, I. *J. Mater. Chem. A* **2013**, *1*, 73.
(20) Zhang, X.; Lu, Z.; Ye, L.; Zhan, C.; Hou, J.; Zhang, S.; Jiang, B.; Zhao, Y.; Huang, J.; Zhang, S.; Liu, Y.; Shi, Q.; Liu, Y.; Yao, J. *Adv. Mater.* **2013**, *25*, 5791.
(21) Lin, Y.; Wang, Y.; Wang, J.; Hou, J.; Li, Y.; Zhu, D.; Zhan, X. *Adv. Mater.* **2014**, *26*, 5137.
(22) Zang, Y.; Li, C.-Z.; Chueh, C.-C.; Williams, S. T.; Jiang, W.; Wang, Z.-H.; Yu, J.-S.; Jen, A. K. Y. *Adv. Mater.* **2014**, *26*, 5708.
(23) Liu, Y.; Mu, C.; Jiang, K.; Zhao, J.; Li, Y.; Zhang, L.; Li, Z.; Lai, J. Y. L.; Hu, H.; Ma, T.; Hu, R.; Yu, D.; Huang, X.; Tang, B. Z.; Yan, H. *Adv. Mater.* **2014**, DOI: 10.1002/adma.201404152.
(24) Pushkara Rao, V.; K.-Y. Jen, A.; Caldwell, J. B. *Tetrahedron Lett.* **1994**, *35*, 3849.
(25) Marinado, T.; Hagberg, D. P.; Hedlund, M.; Edvinsson, T.; Johansson, E. M. J.; Boschloo, G.; Rensmo, H.; Brinck, T.; Sun, L.; Hagfeldt, A. *Phys. Chem. Chem. Phys.* **2009**, *11*, 133.
(26) Insuasty, A.; Ortiz, A.; Tigreros, A.; Solarte, E.; Insuasty, B.; Martín, N. *Dyes Pigm.* **2011**, *88*, 385.
(27) Li, Z.; He, G.; Wan, X.; Liu, Y.; Zhou, J.; Long, G.; Zuo, Y.; Zhang, M.; Chen, Y. *Adv. Energy Mater.* **2012**, *2*, 74.
(28) Zhou, J.; Zuo, Y.; Wan, X.; Long, G.; Zhang, Q.; Ni, W.; Liu, Y.; Li, Z.; He, G.; Li, C.; Kan, B.; Li, M.; Chen, Y. *J. Am. Chem. Soc.* **2013**, *135*, 8484.
(29) Zhou, J.; Wan, X.; Liu, Y.; Zuo, Y.; Li, Z.; He, G.; Long, G.; Ni, W.; Li, C.; Su, X.; Chen, Y. *J. Am. Chem. Soc.* **2012**, *134*, 16345.
(30) Liu, Y.; Chen, C.-C.; Hong, Z.; Gao, J.; Yang, Y.; Zhou, H.; Dou, L.; Li, G. *Sci. Rep* **2013**, *3*, 3356.
(31) Kim, Y.; Song, C. E.; Moon, S.-J.; Lim, E. *Chem. Commun.* **2014**, *50*, 8235.
(32) Siddiki, M. K.; Li, J.; Galipeau, D.; Qiao, Q. *Energy Environ. Sci.* **2010**, *3*, 867.
(33) Leach, S.; Vervloet, M.; Desprès, A.; Bréheret, E.; Hare, J. P.; John Dennis, T.; Kroto, H. W.; Taylor, R.; Walton, D. R. M. *Chem. Phys.* **1992**, *160*, 451.
(34) Muccini, M. *Synth. Met.* **1996**, *83*, 213.
(35) Liu, T.; Troisi, A. *Adv. Mater.* **2013**, *25*, 1038.
(36) Dimitrov, S. D.; Bakulin, A. A.; Nielsen, C. B.; Schroeder, B. C.; Du, J.; Bronstein, H.; McCulloch, I.; Friend, R. H.; Durrant, J. R. *J. Am. Chem. Soc.* **2012**, *134*, 18189.
(37) Kamm, V.; Battagliarin, G.; Howard, I. A.; Pisula, W.; Mavrinskiy, A.; Li, C.; Müllen, K.; Laquai, F. *Adv. Energy Mater.* **2011**, *1*, 297.
(38) Yan, Q.; Zhou, Y.; Zheng, Y.-Q.; Pei, J.; Zhao, D. *Chem. Sci.* **2013**, *4*, 4389.
(39) Bannock, J. H.; Krishnadasan, S. H.; Nightingale, A. M.; Yau, C. P.; Khaw, K.; Burkitt, D.; Halls, J. J. M.; Heeney, M.; de Mello, J. C. *Adv. Funct. Mater.* **2013**, *23*, 2123.
(40) Sun, Y.; Seo, J. H.; Takacs, C. J.; Seifter, J.; Heeger, A. J. *Adv. Mater.* **2011**, *23*, 1679.
(41) Xu, Z.; Chen, L.-M.; Yang, G.; Huang, C.-H.; Hou, J.; Wu, Y.; Li, G.; Hsu, C.-S.; Yang, Y. *Adv. Funct. Mater.* **2009**, *19*, 1227.
(42) Jamieson, F. C.; Domingo, E. B.; McCarthy-Ward, T.; Heeney, M.; Stingelin, N.; Durrant, J. R. *Chem. Sci.* **2012**, *3*, 485.
(43) Ayzner, A. L.; Doan, S. C.; Tremolet de Villers, B.; Schwartz, B. J. *J. Phys. Chem. Lett.* **2012**, *3*, 2281.
(44) Credgington, D.; Durrant, J. R. *J. Phys. Chem. Lett.* **2012**, *3*, 1465.
(45) Mott, N. F.; Gurney, R. W. *Electronic processes in ionic crystals*; Clarendon Press: Oxford, 1948.
(46) Zeman, M.; Krc, J. *J. Mater. Res.* **2008**, *23*, 889.
(47) Kirchartz, T. *Beilstein J. Nanotechnol.* **2013**, *4*, 180.
(48) Dacuña, J.; Salleo, A. *Phys. Rev. B: Condens. Matter* **2011**, *84*, 195209.
(49) Kirchartz, T.; Pieters, B. E.; Kirkpatrick, J.; Rau, U.; Nelson, J. *Phys. Rev. B: Condens. Matter* **2011**, *83*, 115209.
(50) Frost, J. M.; Kirkpatrick, J.; Kirchartz, T.; Nelson, J. *Faraday Discuss.* **2014**, 174.
(51) Campoy-Quiles, M.; Ferenczi, T.; Agostinelli, T.; Etchegoin, P. G.; Kim, Y.; Anthopoulos, T. D.; Stavrinou, P. N.; Bradley, D. D. C.; Nelson, J. *Nat. Mater.* **2008**, *7*, 158.
(52) Schroeder, B. C.; Li, Z.; Brady, M. A.; Faria, G. C.; Ashraf, R. S.; Takacs, C. J.; Cowart, J. S.; Duong, D. T.; Chiu, K. H.; Tan, C.-H.; Cabral, J. T.; Salleo, A.; Chabinyc, M. L.; Durrant, J. R.; McCulloch, I. *Angew. Chem., Int. Ed.* **2014**, *53*, 12870.

DOI: 10.1021/ja5110602
J. Am. Chem. Soc. 2015, 137, 898−904